



Impact of GO on Non-stoichiometric $\text{Mg}_{0.85}\text{K}_{0.3}\text{Fe}_2\text{O}_4$ Ferrite Nanoparticles

Ebtesam E. Ateia¹ · Asmaa Abd Allah¹ · Rania Ramadan¹

Received: 8 April 2022 / Accepted: 20 June 2022 / Published online: 8 July 2022
© The Author(s) 2022

Abstract

Graphene oxide (GO) nanostructures are systems with many fascinating novel properties that can be used to study new science and have significant promise for applications. In this study, graphene oxide was prepared using the modified Hummer's method. In addition, potassium ferrite is a good candidate for biomedical application, as iron and potassium are biocompatible and non-toxic materials. $\text{Mg}_{0.85}\text{K}_{0.3}\text{Fe}_2\text{O}_4/\text{GO}$ nanocomposites were prepared by the citrate auto-combustion method. The effect of adding GO to $\text{Mg}_{0.85}\text{K}_{0.3}\text{Fe}_2\text{O}_4$ on structure, morphology, electrical, and magnetic properties was discussed. Samples under investigation were characterized using XRD, infrared spectroscopy (IR), high-resolution transmission electron microscopy (HRTEM), and atomic force microscopy (AFM). The crystallite size of prepared samples was decreased from 28.098 to 18.148 nm by increasing GO content. Scanning electron microscope (SEM) confirms the successful adhesion of $\text{Mg}_{0.85}\text{K}_{0.3}\text{Fe}_2\text{O}_4$ nanoparticles on graphene oxide sheets, which are dispersed in a metal oxide matrix. EDAX analysis confirms the existence of C, O, K, Mg, and Fe elements present in the samples. Magnetic properties were studied by VSM and Faraday's method. GO has a significant effect on the magnetic properties of nanocomposites. For instance, the saturation magnetization and Curie temperature have diverse values, which will be appropriate for numerous applications.

Keywords Nanoferrites · Graphene oxide · Nanocomposites · Magnetic and electric properties

1 Introduction

Nowadays, nanocrystalline materials have become a very vital and active research subject owing to their rapidly developing in manufacturing sectors and spreading to almost every field of science from engineering to medical [1]. Spinel ferrites (MFe_2O_4 ; $M = \text{Ni, Co, and Mn}$) represent a significant class of magnetic materials however their uses for biomedical applications are disadvantaged because of the high inherent poisonousness of these metals [2]. So, the necessity of synthesis biofavorable nanoferrite is essential. Potassium ferrite is a good candidate for this application, as iron and potassium are biocompatible and non-toxic materials [3]. Magnesium ferrite is an n-type semiconductor material with a spinel structure [4, 5]. Consequently, it has been applied in many fields as sensors, photocatalysts, and anode materials [6–9]. However, nanoscale ferrites have

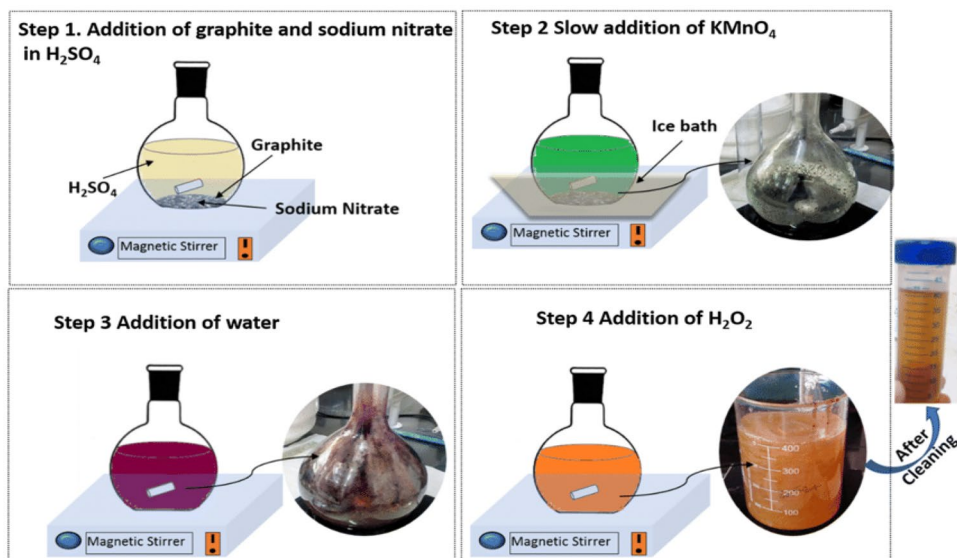
some drawbacks such as the agglomeration of nanoparticles affecting its applications [10]. GO is considered as mass-production of graphene-based materials with large specific surface area, and good bio-compatibility [11, 12]. In recent, the combination of nanoferrites with graphene oxide (GO) has attracted considerable attention due to their desirable properties comparable with their individual counter parts which have excellent properties for biomedical, condensed matter, energy storage as well as water treatment applications [13]. Graphene oxide nanosheets are exfoliated and decorated with nanoferrites [14]. Researchers have keened their efforts to synthesize and study GO/nanoferrite nanocomposites [15].

Herein, the present study is aimed at synthesizing and characterization of GO-based spinel ferrites ($\text{Mg}_{0.85}\text{K}_{0.3}\text{Fe}_2\text{O}_4$) nanoparticles by the citrate auto-combustion method. The structural, optical, electrical, and magnetic properties of the prepared samples are studied. Also, one of our goals is to reach the critical concentration at which the physical properties reach their optimum values and the sample becomes more applicable.

✉ Ebtesam E. Ateia
drebtesam2000@yahoo.com; ebtesam@sci.cu.edu.eg

¹ Physics Department, Faculty of Science, Cairo University, 12613 Giza, Egypt

Fig. 1 GO was developed in a standard procedure using modified method of hummers from pure graphite powder



2 Experimental

2.1 Preparation of Graphene Oxide (GO)

Graphene oxide (GO) [16] was developed in a standard procedure using a modified method of hummers from pure graphite

powder as shown in Fig. 1. Oxidation of graphite was carried out by mixing sodium nitrate sulfuric acid H_2SO_4 , with graphite powder using a magnetic stirrer. The mixture was transferred to a 250-mL beaker and cooled in an ice bath. With vigorous stirring, the potassium permanganate ($KMnO_4$) was gradually added to the solution. To eliminate excess $KMnO_4$,

Fig. 2 Flowchart of preparation method

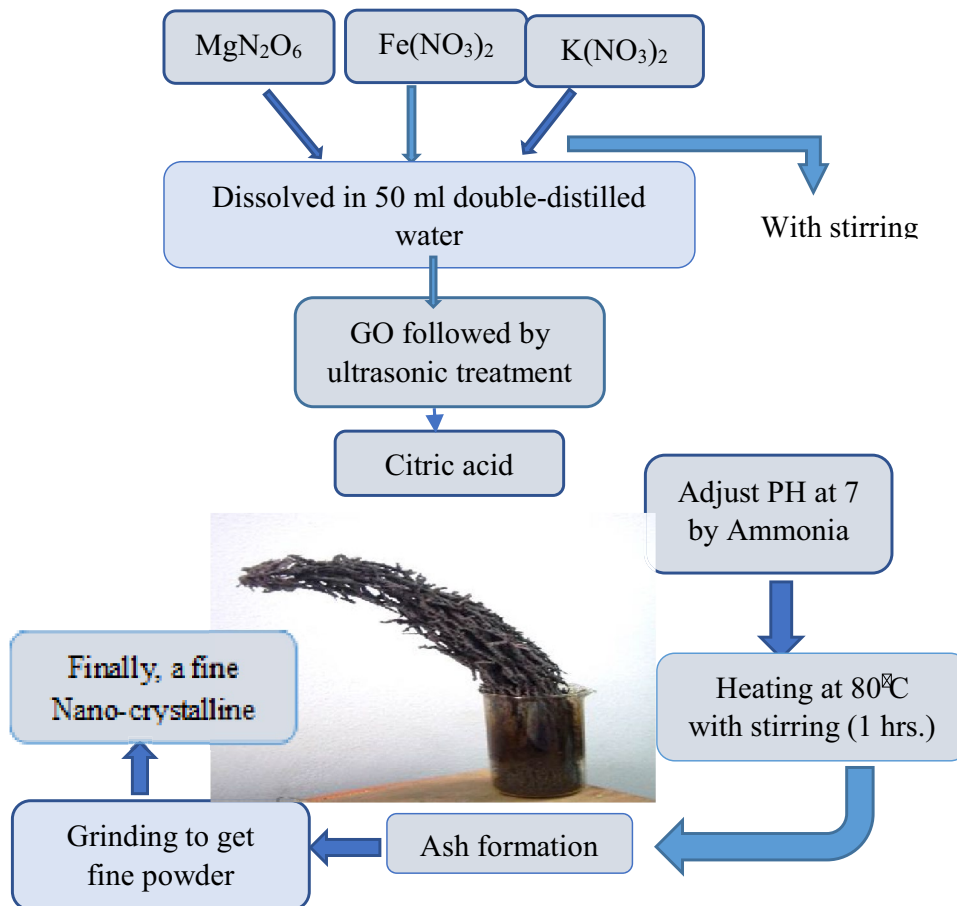
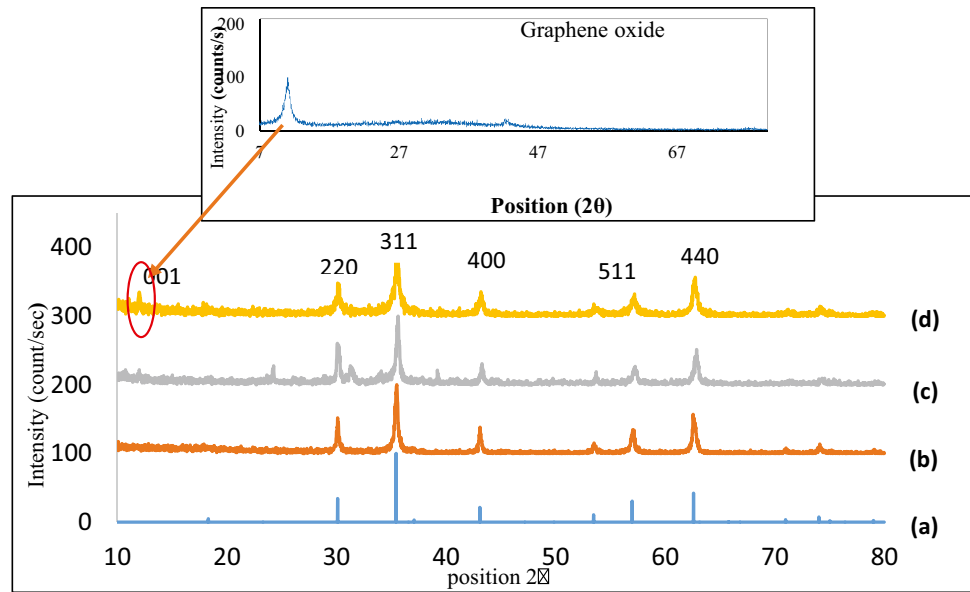


Fig. 3 The X-ray diffraction pattern for **a** card, **b** $\text{Mg}_{0.85}\text{K}_{0.3}\text{Fe}_2\text{O}_4$, **c** GO (1%)/ $\text{Mg}_{0.85}\text{K}_{0.3}\text{Fe}_2\text{O}_4$, and **d** GO (10%)/ $\text{Mg}_{0.85}\text{K}_{0.3}\text{Fe}_2\text{O}_4$



hydrogen peroxide (H_2O_2) was progressively reduced and agitated for 10 min. It cooled down as a result of the exothermic process. The Eppendorf Centrifuge 5430R was used to centrifuge 10 mL of hydrochloric acid (HCl) and 30 mL of deionized water (DIW) at 5000 rpm for 7 min. After decanting the supernatant, the residuals were rewashed three times with HCl and DIW. To make GO powder, the cleaned GO solution was completely dried.

2.2 Sample Preparation of GO (1%, 10%) + $\text{Mg}_{0.85}\text{K}_{0.3}\text{Fe}_2\text{O}_4$ Ferrite Nanoparticles

The citrate auto-combustion method was used for the preparation of the investigated samples. Under magnetic stirring, a non-stoichiometric amount of magnesium nitrate (II) ($\text{Mg}(\text{NO}_3)_2 \cdot 6\text{H}_2\text{O}$), potassium ($\text{K}(\text{NO}_3)0.6\text{H}_2\text{O}$), and iron (III) nitrate ($\text{Fe}(\text{NO}_3)_3 \cdot 9\text{H}_2\text{O}$) was dissolved in 50 mL of

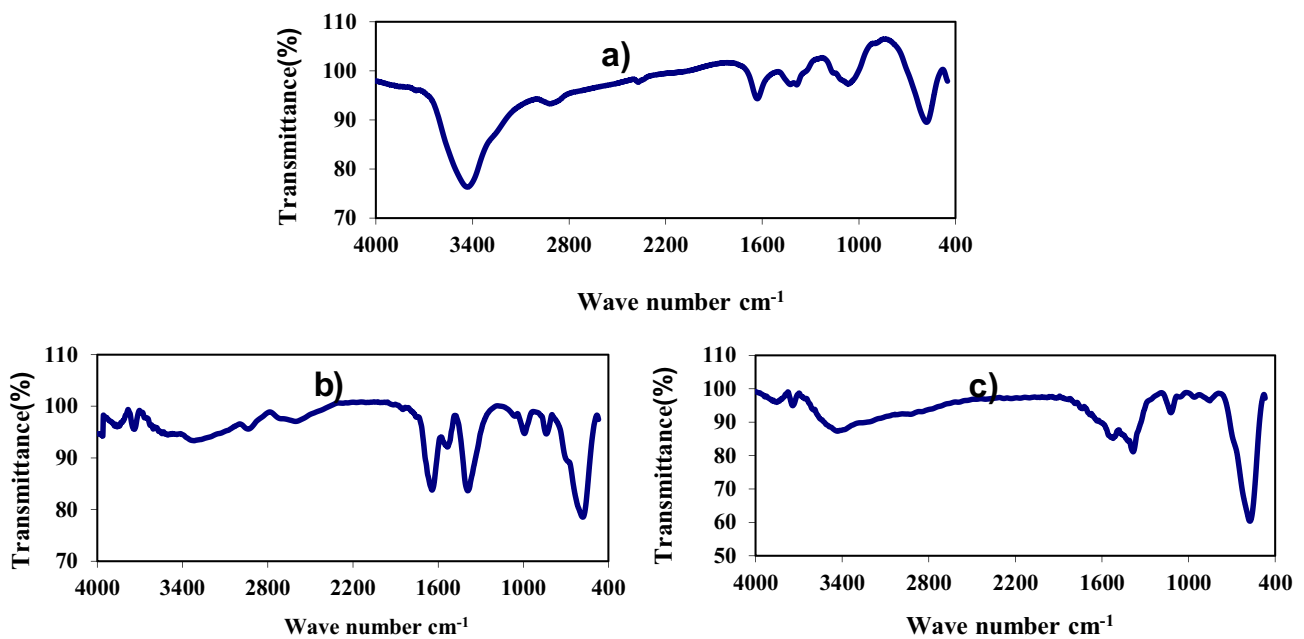


Fig. 4 FTIR for **a** $\text{Mg}_{0.85}\text{K}_{0.3}\text{Fe}_2\text{O}_4$, **b** GO (1%)/ $\text{Mg}_{0.85}\text{K}_{0.3}\text{Fe}_2\text{O}_4$, and **c** GO (10%)/ $\text{Mg}_{0.85}\text{K}_{0.3}\text{Fe}_2\text{O}_4$

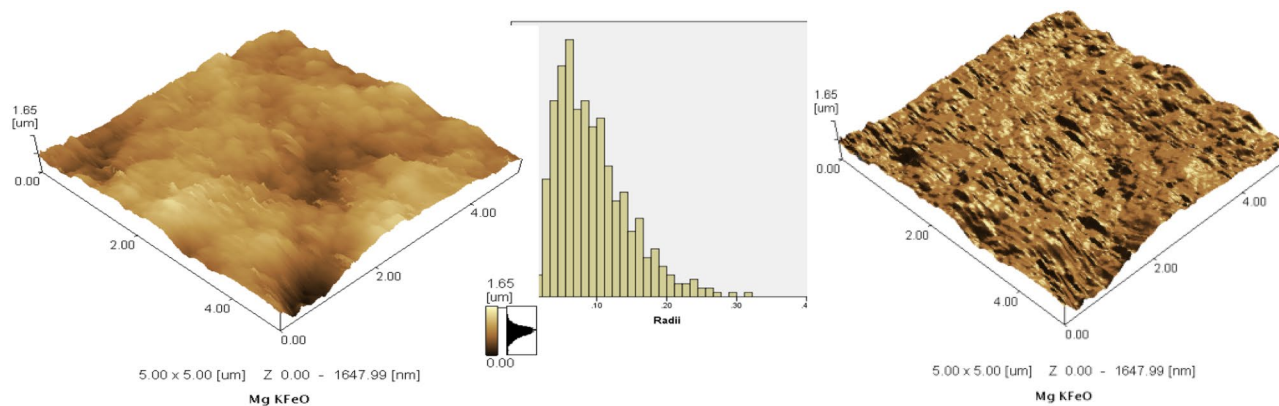


Fig. 5 Atomic force microscopy (AFM) image of nano-GO/Mg_{0.85}K_{0.3}Fe₂O₄

double-distilled water. Then, different wt % of GO (1 wt%, 10 wt%) were added to the solution, followed by ultrasonic treatment for about 1 h until GO was well dispersed in the solution. To improve homogeneous mixing, citric acid (C(OH)(COOH)(CH₂COOH)₂H₂O) was used. The molar ratio of cations/citric acid was maintained at 1:1. The solution was continuously stirred for 1 h. Meanwhile, NaOH solution (0.5 mol/L) was added dropwise into the above solution to regulate the pH value of the mixed solution to 7. The obtained precursor solution was then heated on a hot plate at 80 °C with constant stirring until it began to evolve reddish brown colored gases and transform into a highly viscous gel. Finally, the dried gel was finally burnt-out completely to form loose powder. The procedure of the preparation was illustrated in the following chart (Fig. 2).

X-ray diffractometer (XRD) and Fourier-transform infrared (FTIR) spectra were used to ratify the crystallinity and structure of the samples. Morphology of the prepared samples was studied by high-resolution transmission electron microscopy (HRTEM) and atomic force microscopy (AFM). Magnetic properties of samples were discussed through the vibration sample magnetometer (model 9600–1 LDJ, USA) (VSM) as well as Faraday’s method. Electrical conductivity was studied as a function of temperature and frequencies by the LCR bridge (Hioki 3532, Japan).

3 Results and Discussion

3.1 Structural Analyses

Figure 3 represents the XRD pattern of Mg_{0.85}K_{0.3}Fe₂O₄ with 0.0, 1%, and 10% of GO. The investigated diffraction peaks DP_s are located at 30.213°, 35.589°, 43.254°, 57.211°, and 62.832°. The detected peaks are related to (220), (311), (400), (511), and (440) crystal planes of MgFe₂O₄. The XRD patterns (Fig. 3c, d) of 1% GO/Mg_{0.85}K_{0.3}Fe₂O₄

nanoparticles and 10% GO/Mg_{0.85}K_{0.3}Fe₂O₄ nanoparticles are nearly identical, with peaks of cubic spinel ferrite and a very small peak of GO.

In XRD patterns of the prepared ferrite nanoparticles, the main DP_s can be assigned to the cubic spinel structure card no. (01–088-1938). On the other hand, the chart of GO (inset of the Fig. 3) exhibits a 001 reflection peak at 12.0° with a basal spacing of *d* (001). It is approximately equal to 8.03 Å according to the Bragg equation which confirms the formation of GO.

However, the DP_s of GO are not clearly identified for the prepared samples. This can be attributed to the addition of a small amount of graphene during the synthesis process as well as the low-diffraction intensity of GO sheets [17]. The crystallite size “*L*” of the prepared samples is calculated using the Scherrer equation as mentioned in the previous work [18].

An additional tool for the characterization of GO/Mg_{0.85}K_{0.3}Fe₂O₄ is FTIR spectroscopy. Figure 4 displays the IR pattern of Mg_{0.85}K_{0.3}Fe₂O₄, GO (1%)/Mg_{0.85}K_{0.3}Fe₂O₄, and GO (10%)/Mg_{0.85}K_{0.3}Fe₂O₄ nanoparticles in the range between 400 and 4000 cm⁻¹. A peak of around 3500 cm⁻¹ for all the spectra is related to the stretching vibration (SV) of O–H in adsorbed water molecules [19]. The peak at 1550 cm⁻¹ can be attributed to the formation of COO₂ after decorating with Mg_{0.85}K_{0.3}Fe₂O₄. The specific peak at 590 is related to the SV of the Fe–O band. From the mentioned results, one can demonstrate that GO is bonded to spinel nanoparticles through a covalent bond [20].

Table 1 The crystallite size (*L*) of the investigated samples

Sample	Crystallite size “ <i>L</i> ”
Mg _{0.85} K _{0.3} Fe ₂ O ₄	28.098
GO (1%) + Mg _{0.85} K _{0.3} Fe ₂ O ₄	25.337
GO (10%) + Mg _{0.85} K _{0.3} Fe ₂ O ₄	18.148

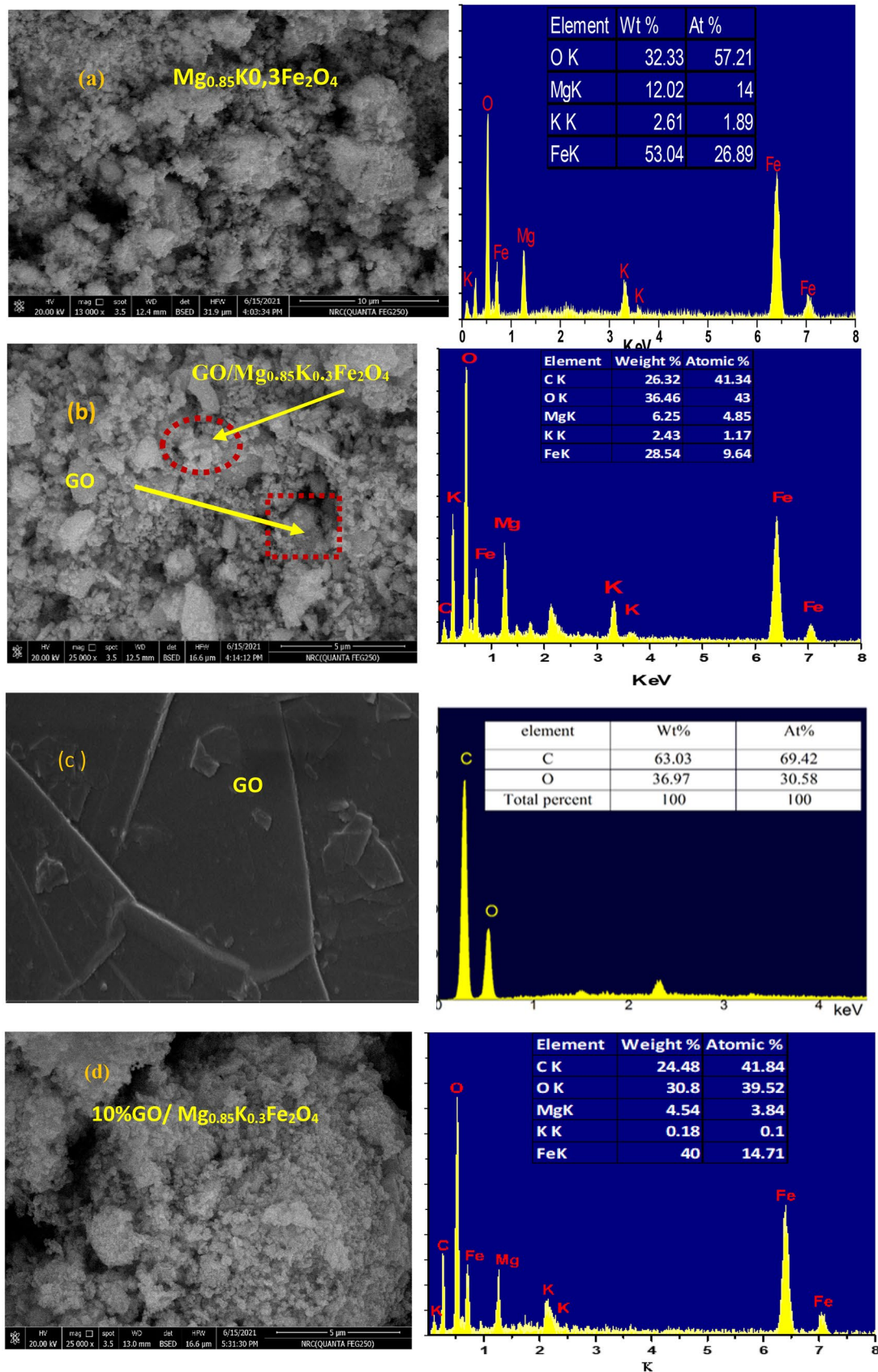


Fig. 6 SEM micrographs and EDAX spectra for **a** $Mg_{0.85}K_{0.3}Fe_2O_4$, **b** $GO(1\%)/Mg_{0.85}K_{0.3}Fe_2O_4$, **c** GO, and **d** $GO(10\%)/Mg_{0.85}K_{0.3}Fe_2O_4$

The IR spectra of GO indicate a broad and strong peak around 3400 cm^{-1} matching the SV of hydroxyl “OH” groups. The additional peaks at 1040 cm^{-1} , 1224 cm^{-1} , 1494 , and 1785 cm^{-1} correspond to C–O stretching, C–OH stretching, C–O–H bending, and C–O stretching vibrations of carboxyl (COOH) groups. The peak at 1619 cm^{-1} is

related to aromatic C–C indicating the hybrid sp^2 structure of graphene.

Finally, the results of XRD and FT-IR spectra verify that the nanocomposites are formed in the synthesis.

Figure 5 shows AFM of $\text{Mg}_{0.85}\text{K}_{0.3}\text{Fe}_2\text{O}_4$. Quantitative information such as surface area, particle size, and surface

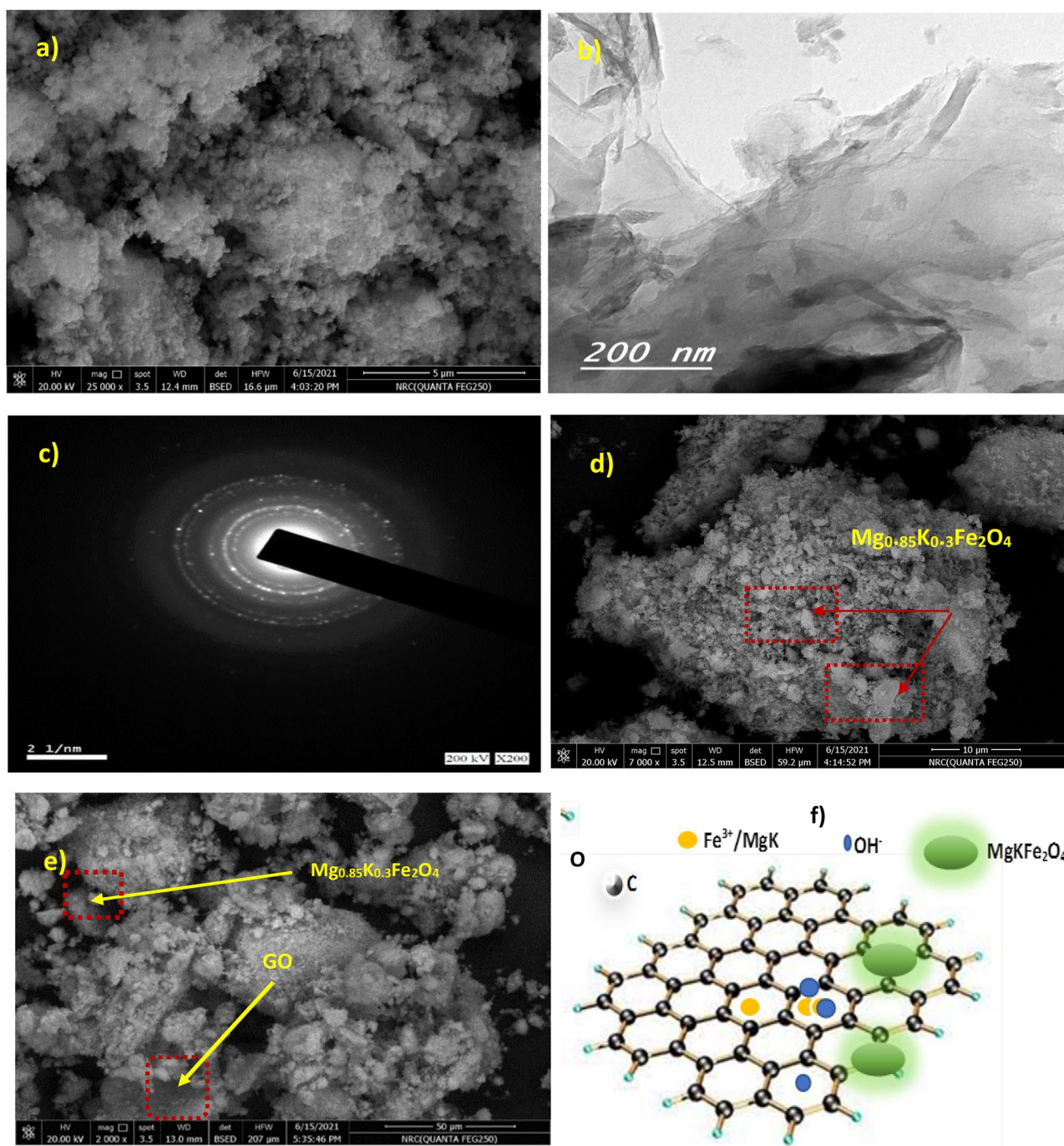
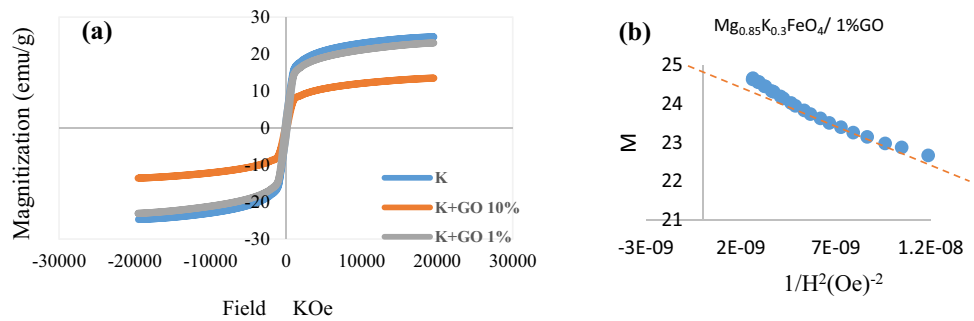


Fig. 7 a–f HRTEM micrograph with the histogram for The HRTEM image for **a** $\text{Mg}_{0.85}\text{K}_{0.3}\text{Fe}_2\text{O}_4$, **b** is the HRTEM for graphene oxide, **c** selected region (SAED) of the samples **d** GO (1%)/ $\text{Mg}_{0.85}\text{K}_{0.3}\text{Fe}_2\text{O}_4$, **e** GO (10%)/ $\text{Mg}_{0.85}\text{K}_{0.3}\text{Fe}_2\text{O}_4$, and **f** schematic represent the decoration

Fig. 8 **a** The hysteresis loops of the investigated samples using a vibrating sample magnetometer (VSM). **b** Fitting plot between M versus $1/H^2$ for the investigated samples



roughness are calculated from atomic force microscopy (AFM) software and listed in Table 1.

Atomic force microscopy images of the single-layer flakes show high-quality graphene oxide with well-defined edges and a relatively low amount of surface defects in the form of cracks and wrinkles.

Figure 6a–f shows the scanning electron micrographs (SEM) and energy dispersive spectra (EDAX) for the investigated samples. The agglomeration of ferrite nanoparticles can be well detected. This agglomeration is attributed to the high surface energy and magnetic interaction between the nanocrystallites.

The SEM images of the prepared $\text{Mg}_{0.85}\text{K}_{0.3}\text{Fe}_2\text{O}_4$ display a narrow-size distribution at a large-scale. In addition, it is noticed that the auto combustion synthesis technique produces highly monodispersed nanospheres of $\text{Mg}_{0.85}\text{K}_{0.3}\text{Fe}_2\text{O}_4$ with an average size of about 45 nm.

EDAX assigns the hidden elements and impurities in the samples with their atomic (At) and weight (Wt) percentages of constituent elements (C, Mg, K, Fe, and O) as illustrated in the inset of the figure. No impurities are detected in the EDAX spectrum, confirming the purity of synthesized samples.

As shown from Fig. 6e, carbon and oxygen are present in the pure GO sample, which approves the purity of the investigated material. The carbon peaks that are not noticeable in the XRD diagram (Fig. 3) can be easily detected in EDAX data.

HRTEM images of $\text{Mg}_{0.85}\text{K}_{0.3}\text{Fe}_2\text{O}_4$, 1% GO/ $\text{Mg}_{0.85}\text{K}_{0.3}\text{Fe}_2\text{O}_4$, and 10% GO/ $\text{Mg}_{0.85}\text{K}_{0.3}\text{Fe}_2\text{O}_4$ NPs are shown in Fig. 7a–f. The surface of the specimens is smooth with a cubic shape. Figure 7b depicts the HRTEM image of the GO sheets, which have multilayered structures and rough texture as seen in the figure. Along with some wrinkles and folds, the GO sheet possesses a large aspect ratio, which may be the chief parameter behind the strengthening of the contact area with ferrite. The configuration of the selected region

(SAED) is illustrated in Fig. 7c. The image clearly demonstrates a bright dot layout that confirms the nano-structure characteristic of the samples. The corresponding SAED pattern displays diffraction rings, corresponding to the planes (111), (220), and (311) and confirming the polycrystalline nature of the $\text{Mg}_{0.85}\text{K}_{0.3}\text{Fe}_2\text{O}_4/\text{GO}$ ferrite NPs. The agglomeration of the particles is detected in the HRTEM image. This can be attributed to the collision and the amalgamation between the NPs.

The images of $\text{Mg}_{0.85}\text{K}_{0.3}\text{Fe}_2\text{O}_4/\text{GO}$ NPs Fig. 7e show that the $\text{Mg}_{0.85}\text{K}_{0.3}\text{Fe}_2\text{O}_4$ NPs are decorated homogeneously on flake-like GO sheets. This decoration can be represented in the schematic figure (Fig. 7f). The HRTEM data are consistent with the previously mentioned XRD results.

3.2 Magnetic Properties

3.2.1 Hysteresis Loop and Magnetic Parameters

Generally, there are no nonmagnetic materials, and even if the effect is very small, diamagnetism is inherent to all materials. Numerous types of carbon allotropes display diamagnetic susceptibility χ at room temperature RT [21].

Figure 8 shows the hysteresis loops of the investigated samples at 300 K and the fitted Langevin plot. It is clear that the magnetization for all investigated samples increases with the applied magnetic field until reaching saturation behavior. A weak ferromagnetic behavior with narrow loops is detected for the pure and doped samples. However, the incorporation of GO into the $\text{Mg}_{0.85}\text{K}_{0.3}\text{Fe}_2\text{O}_4$ nanoparticles increases the cation redistribution, changes the morphology, increases surface roughness, and decreases the crystallite sizes of the investigated samples [22]. It has been shown theoretically [22] and experimentally [23] that defects lead to an increase in the magnetic moment of graphene. These changes are related to the increase of unpaired spins.

Table 2 Surface area and surface roughness of nano-GO/ $\text{Mg}_{0.85}\text{K}_{0.3}\text{Fe}_2\text{O}_4$

Sample	Surface area	Surface roughness	Particle size (nm)
GO/ $\text{Mg}_{0.85}\text{K}_{0.35}\text{Fe}_2\text{O}_4$	0.048	1.721	28.098

Table 3 The saturation magnetization M_s , remnant magnetization (M_r) and coercivity (H_c), squareness (M_r/M_s), and magnetic moment (n_B), anisotropy constant K , and exchange bias field H_{exch} of the prepared samples

Sample	M_s (emu/g)	H_c (Oe)	M_r	M_r/M_s	n_B	K (emu Oe.g ⁻¹)	H_{exch} (Oe)
$Mg_{0.85}K_{0.3}Fe_2O_4$	24.672	109	1.904	0.077	0.919	2807	9.610
1%GO/ $Mg_{0.85}K_{0.3}Fe_2O_4$	23.032	138	2.309	0.100	0.858	3238	6.630
10% GO/ $Mg_{0.85}K_{0.3}Fe_2O_4$	13.514	95	0.801	0.059	0.503	1310	30.926

Another source of magnetic moments and magnetic ordering of the GO can be derived from the localized edge states of graphene. First principles and mean-field theory calculations have shown that carbon structures that consist of zigzag edges can be magnetic [24]. Theoretical calculations show that localized electron spins in zigzag ribbons are polarized, resulting in ferromagnetism [25].

By increasing the amount of GO, saturation magnetization (M_s) decreases from 24.672 to 13.514 emu/g. This may be related to the decrease in particle size when $Mg_{0.85}K_{0.3}Fe_2O_4$ is distributed on the GO surface, aside from the diamagnetic behavior of the graphene oxide. The small values obtained of remnant magnetization (M_r) and coercivity (H_c) for $Mg_{0.85}K_{0.3}Fe_2O_4/GO$ are desirable for many practical applications that require strong magnetic signals at small applied magnetic fields.

The M_s values that correspond to 20 kOe is 24.672 emu/g. The M_s of $Mg_{0.85}K_{0.3}Fe_2O_4$ nanoparticle can also be noticed using the Stoner–Wohlfarth theory by extrapolating the plot of magnetization versus $1/H^2$ to approach 0 [26, 27]. This

theory is applied to non-interacting particles as approved by the M_r/M_s values in Table 2. In this way, the M_s value is equal to 25 emu/g. The estimated and investigational values are comparable with each other, signifying that the field of ± 20 kOe is fitting to saturate the testified samples.

All magnetic parameters as M_s , H_c , M_r , squareness (M_r/M_s), and magnetic moment (n_B) are tabulated in Table 3. The types of inter grain group exchanges can be detected from M_r/M_s values [28].

Herein, the ratio between (M_r/M_s) is listed in Table 3, which means that the samples have magneto static interactions. Anisotropy constant K is obtained from the following equation [7]:

$$H_c = \frac{0.98K}{M_s} \quad (1)$$

The addition of GO causes a noticeable shift of the magnetic loop that is ascribed to exchange bias phenomena.

The exchange bias field is estimated from Eq. (3) and tabulated in Table 3.

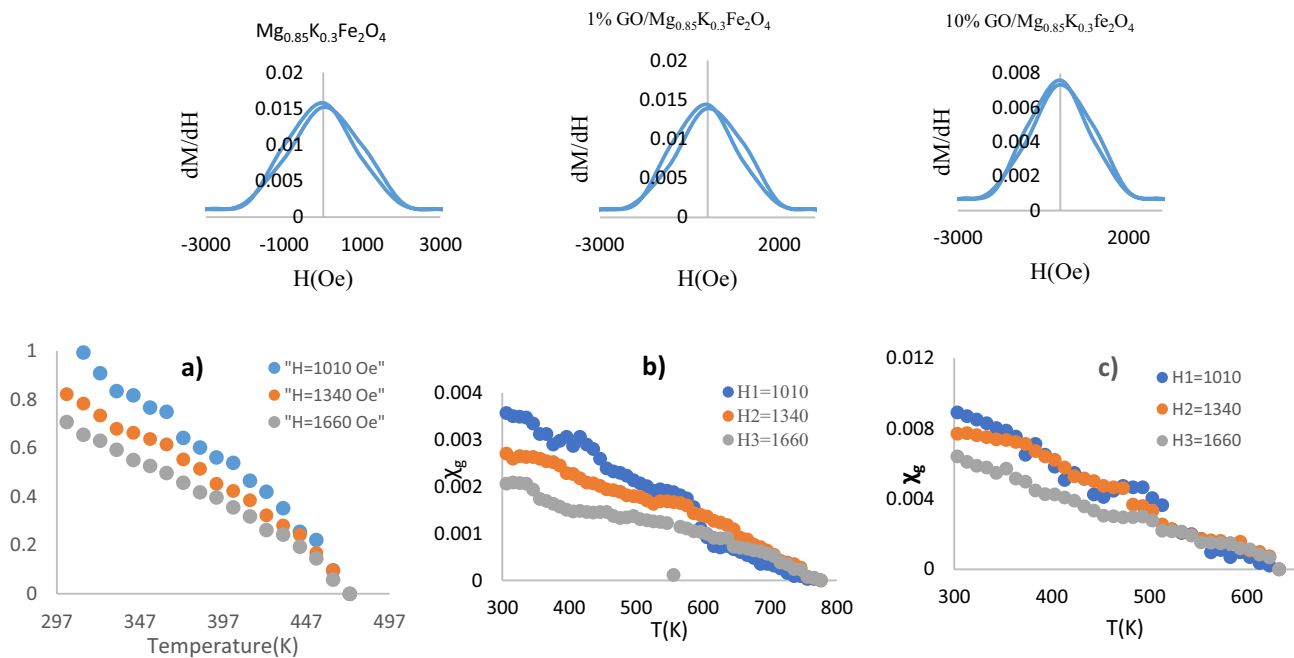
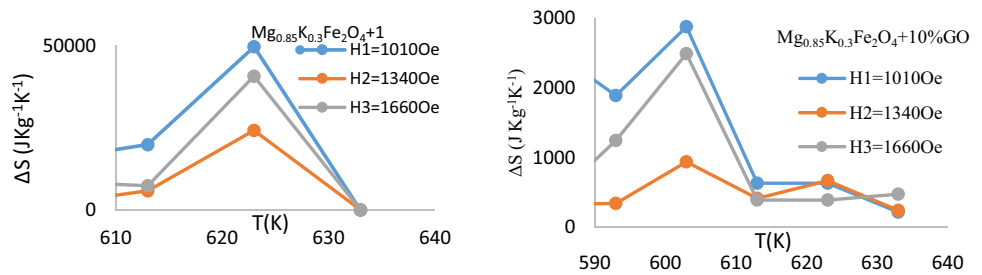
**Fig. 9** SFD value for the investigated samples as a function of magnetic field. **a** $Mg_{0.85}K_{0.3}Fe_2O_4$, **b** GO (0.57%) + $Mg_{0.85}K_{0.3}Fe_2O_4$, and **c** GO (10%) + $Mg_{0.85}K_{0.3}Fe_2O_4$

Fig. 10 The change of entropy with temperature for $\text{Mg}_{0.85}\text{K}_{0.3}\text{Fe}_2\text{O}_4/1\% \text{GO}$ and $\text{Mg}_{0.85}\text{K}_{0.3}\text{Fe}_2\text{O}_4/10\%$, at different magnetic fields



$$H_{\text{exch}} = \frac{-(H_{\text{left}} + H_{\text{right}})}{2} \quad (2)$$

The exchange bias values confirm the presence of various spin configurations. In the nanostructure sample, the magnetic structure of the core is numerous from that of the surface where spin frustration predominates [29, 30].

The size of the NPs has a crucial role in the magnetization of the samples. From the previous discussion in structure analysis, the decrease of the particle size D with increasing content of GO leads to a decrease in M_s as illustrated in the Table 3. This can be attributed to the existence of the GO layers that reduce the magneto crystalline and surface anisotropy and introduce shape and stress anisotropy due to the wrinkle layered nature of GO [31, 32]. The overall competition between the above-mentioned anisotropies reduces the anisotropy constant K as well as H_c in Eq. (1).

On the other hand, the smaller particle size of $\text{GO}/\text{Mg}_{0.85}\text{K}_{0.3}\text{Fe}_2\text{O}_4$ increases the inert layer, causing “ M_s ” to decrease. Furthermore, the surface enhanced property of GO, intensifying the surface energy of the carriers. As a result, the magneto-static energy of the ferrite decreases [33]. Accordingly, the exchange in the cationic preference, the increase in the anti-site defects, and the decrease in the “ M_s ” are expected. This property of the materials enables the magnetization of the GO-doped samples to take place at a faster rate with a lower applied field [34]. This feature makes the examined samples suitable for high-frequency devices, data storage devices, and erasable memories.

The switching field distribution (SFD) for the samples is one of the important standards for high-density recording performance [35].

Figure 9 shows the SFD value for the 1% $\text{GO}/\text{Mg}_{0.85}\text{K}_{0.3}\text{Fe}_2\text{O}_4$ and 10% $\text{GO}/\text{Mg}_{0.85}\text{K}_{0.3}\text{Fe}_2\text{O}_4$ as a function of coercivity. The SFD value is estimated from Eq. (3) as the ratio of the $1/2$ width of the peak of $\partial M/\partial H$ and the magnetic field plot.

$$SFD = \frac{\Delta H}{H_c} \quad (3)$$

The present plot displays a double peak (DP) typical of a two-step reversal. Commonly, the DP reveals the competition between exchange coupling and strong dipolar

interactions [36–38]. In the case study, the dipolar interactions are more effective, for the testified samples, which implies a strong reduction of the inter bump exchange coupling in our bump array.

3.2.2 Magnetic Susceptibility

The molar magnetic susceptibility (χ) as a function of absolute temperature at three different field intensities is illustrated in Fig. 10a–c. For all studied samples, χ decreases with increasing temperature until it reaches to 0 at the Curie temperature T_c .

This can be attributed to the increase in the thermal energy of the system, increasing the disturbance of the dipoles. At T_c , a complete disorder is taking place and samples are transformed from ferromagnetic into paramagnetic phases [39].

The addition of GO has a great effect on the Curie temperature of the investigated samples, as shown from Table 4. The distribution of $\text{Mg}_{0.85}\text{K}_{0.3}\text{Fe}_2\text{O}_4$ nanoparticles on the GO surface decreases the spin disorder. Consequently, the domains become well-oriented [40] and the ferromagnetic region becomes wider compared to the paramagnetic one.

The maximum magnetic entropy change $\Delta S(T, H)$ of $\text{Mg}_{0.85}\text{K}_{0.3}\text{Fe}_2\text{O}_4$ and $\text{Mg}_{0.85}\text{K}_{0.3}\text{Fe}_2\text{O}_4/\text{GO}$ is determined from the magnetization data in the temperature range from 300 to 800 K and by the use of the Maxwell equations as follows [41]:

$$\Delta S_M = \int_{H_i}^{H_f} \frac{\partial M}{\partial T} dH \quad (4)$$

Table 4 Curie temperature of the prepared samples

Sample	T_c (K)	T_c from entropy (K)
$\text{Mg}_{0.85}\text{K}_{0.3}\text{Fe}_2\text{O}_4$	454	–
$\text{GO (1%)/Mg}_{0.85}\text{K}_{0.3}\text{Fe}_2\text{O}_4$	776	623
$\text{GO (10%)/Mg}_{0.85}\text{K}_{0.3}\text{Fe}_2\text{O}_4$	633	603

$$|\Delta S_M| = \sum_i \frac{M_i - M_{i+1}}{T_{i+1} - T_i} \Delta H_i \quad (5)$$

The change of the magnetic entropy ΔS_M with temperature as a function of magnetic field ($H = 1010, 1340, 1660$ Oe) is revealed in Fig. 10. The figure displays a distinctive shape with a maximum change near the Curie temperature, T_c . As shown from the figure, the increase of applied magnetic field (H) increases the ΔS_M of the system. On the other hand, the increase of the GO decreases the disorder and the ΔS_M . This can be clarified as the increase in the H and the content of GO affect the magnetic order of the prepared sample. The calculated T_c from the Curie–Weiss law agrees well with T_c obtained from the maximum ΔS_M as tabulated in Table 4.

4 Conclusion

$Mg_{0.85}K_{0.3}Fe_2O_4/GO$ nanoparticles have been successfully synthesized by the citrate combustion technique. Adding GO displays the varying structures and magnetic properties. The XRD pattern confirms the single spinel structure of the prepared samples.

The Curie temperature increases from 473 to 776 K with increasing GO content while “ M_s ” and “ H_c ” decrease.

The micrographs revealed successful decoration of GO with $Mg_{0.85}K_{0.3}Fe_2O_4$ nanoparticles, with a reduction in particle size.

The massive transition temperature enhancement is demonstrated for the GO-doped samples compared to the pure ones.

5 Future Work

The numerous uses of $Mg_{0.85}K_{0.3}Fe_2O_4/GO$ spinel nanoferrite particles will be the main issue for future work. The main advantages of the synthesized sample are ease of separation, high adsorption, low cost, and recyclable with notable efficiency. Thus, it is suggested as a promising candidate for waste water treatment [42].

The cheap and non-toxic $Mg_{0.85}K_{0.3}Fe_2O_4/GO$ spinel nanoferrite particles can be employed as an anode for lithium-ion batteries (LIBs). It can demonstrate superior electrochemical performance in terms of specific capacity, cycle performance, and rate capability [43].

In addition, potassium ferrite is a good candidate for biomedical application, as iron and potassium are biocompatible and non-toxic materials [44].

Funding Open access funding provided by The Science, Technology & Innovation Funding Authority (STDF) in cooperation with The Egyptian Knowledge Bank (EKB).

Declarations

Competing Interest The authors declare no competing interests.

Open Access This article is licensed under a Creative Commons Attribution 4.0 International License, which permits use, sharing, adaptation, distribution and reproduction in any medium or format, as long as you give appropriate credit to the original author(s) and the source, provide a link to the Creative Commons licence, and indicate if changes were made. The images or other third party material in this article are included in the article's Creative Commons licence, unless indicated otherwise in a credit line to the material. If material is not included in the article's Creative Commons licence and your intended use is not permitted by statutory regulation or exceeds the permitted use, you will need to obtain permission directly from the copyright holder. To view a copy of this licence, visit <http://creativecommons.org/licenses/by/4.0/>.

References

1. Sripriya, R.C., Mahendiran, M., Madahavan, J., Raj, M.V.A.: Enhanced magnetic properties of $MgFe_2O_4$ nanoparticles. *Materials Today: Proceedings* **8**, 310–314 (2019)
2. Khanna, L., Verma, N.K.: Synthesis, characterization and biocompatibility of potassium ferrite nanoparticles. *J. Mater. Sci. Technol.* **30**(1), 30–36 (2014)
3. Ciabatti, I., Tognotti, F., Lombardi, L.: Treatment and reuse of dyeing effluents by potassium ferrate. *Desalination* **250**(1), 222–228 (2010)
4. Ateia, E.E., Mohamed, A.T.: Nonstoichiometry and phase stability of Al and Cr substituted Mg ferrite nanoparticles synthesized by citrate method. *J. Magn. Magn. Mater.* **426**, 217–224 (2017)
5. Jang, H.W., Zareidoost, A., Moradi, M., Abuchenari, A., Bakhtiari, A., Pouriamanesh, R., Malekpouri, B., Rad, A.J., Rahban, D.: Photosensitive nanocomposites: environmental and biological applications. *Journal of Composites and Compounds* **2**(2), 50–60 (2020)
6. Zu, Y., Zhang, Y., Xu, K., Zhao, F.: A graphene oxide– $MgWO_4$ nanocomposite as an efficient catalyst for the thermal decomposition of RDX. *HMX. Rsc Advances* **6**(37), 31046–31052 (2016)
7. Kaur, N., Kaur, M.: Envisioning the composition effect on structural, magnetic, thermal and optical properties of mesoporous $MgFe_2O_4$ -GO nanocomposites. *Ceram. Int.* **44**(4), 4158–4168 (2018)
8. Wang, W., Liu, B., Xu, K., Zu, Y., Song, J., Zhao, F.: In-situ preparation of $MgFe_2O_4$ -GO nanocomposite and its enhanced catalytic reactivity on decomposition of AP and RDX. *Ceram. Int.* **44**(15), 19016–19020 (2018)
9. Alizadeh-Gheshlaghi, E., Shaabani, B., Khodayari, A., Azizian-Kalandaragh, Y., Rahimi, R.: Investigation of the catalytic activity of nano-sized CuO , Co_3O_4 and $CuCo_2O_4$ powders on thermal decomposition of ammonium perchlorate. *Powder Technol.* **217**, 330–339 (2012)
10. Li, J.J., Zhao, Y., Li, H.S., Wu, Q., Jiao, Q.Z.: Preparation of hollow nickel ferrite microspheres and their magnetic properties. In *Advanced Materials Research* **1035**, 488–491 (2014)
11. Ateia, E.E., Mohamed, A.T., Elsayed, K.: Impact of Gd^{3+} /graphene substitution on the physical properties of magnesium ferrite nanocomposites. *J. Magn. Magn. Mater.* **452**, 169–178 (2018)
12. Hou, C., Zhang, Q., Zhu, M., Li, Y., Wang, H.: One-step synthesis of magnetically-functionalized reduced graphite sheets and their use in hydrogels. *Carbon* **49**(1), 47–53 (2011)
13. Ateia, E.E., Abdelamksoud, M.K., Arman, M.M., Ramadan, R., Shafaay, A.S.: Optimizing the physical properties of cobalt/

- graphene nanocomposites for technological applications. *Appl. Phys. A* **125**(8), 1–8 (2019)
14. Bai, S., Shen, X., Zhong, X., Liu, Y., Zhu, G., Xu, X., Chen, K.: One-pot solvothermal preparation of magnetic reduced graphene oxide-ferrite hybrids for organic dye removal. *Carbon* **50**(6), 2337–2346 (2012)
 15. Nethravathi, C., Nisha, T., Ravishankar, N., Shivakumara, C., Rajamathi, M.: Graphene–nanocrystalline metal sulphide composites produced by a one-pot reaction starting from graphite oxide. *Carbon* **47**(8), 2054–2059 (2009)
 16. Nayak, P.K. ed.: Recent advances in graphene research (2016). <https://doi.org/10.5772/61909>
 17. Alves, Z., Nunes, C., Ferreira, P.: Unravelling the role of synthesis conditions on the structure of zinc oxide-reduced graphene oxide nanofillers. *Nanomaterials* **11**(8), 2149 (2021)
 18. Ateia, E.E., Mohamed, A.T.: Core–shell nanoarchitectonics of CoFe_2O_4 encapsulated $\text{La}_2\text{Fe}_2\text{O}_6$ nanoparticles for their use in various applications. *J. Inorg. Organomet. Polym. Mater.* **32**, 1389–1399 (2022)
 19. Hino, M.: Infrared studies on water adsorption systems with the use of HDO. I. Molecular sieves 13X and 4A. *Bull. Chem. Soc. Jpn.* **50**(3), 574–579 (1977)
 20. Koçanalı, A., Apaydın Varol, E.: An experimental study on the electrical and thermal performance of reduced graphene oxide coated cotton fabric. *Int. J. Energy Res.* **45**(9), 12915–12927 (2021)
 21. Bianco, A., Chen, Y., Frackowiak, E., Holzinger, M., Koratkar, N., Meunier, V., Mikhailovsky, S., Strano, M., Díez Tascón, J.M., Terrones, M.: Carbon science perspective. Current research and future challenges (2020)
 22. Yazyev, O.V., Helm, L.: Defect-induced magnetism in graphene. *Phys. Rev. B* **75**, 6 (2007)
 23. Nair, R.R., et al.: Spin-half paramagnetism in graphene induced by point defects. *Nat. Phys.* **8**, 199–202 (2012)
 24. Kuzemsky, A.L.: Unconventional and exotic magnetism in carbon-based structures and related materials. *Int. J. Mod. Phys. B* **27**, 40 (2013)
 25. Tada, K., et al.: Graphene magnet realized by hydrogenated graphene nanopore arrays. *Appl. Phys. Lett.* **99**, 4 (2011)
 26. Chiaracane, C., Pietracaprina, F., Purkayastha, A., Goold, J.: Quantum dynamics in the interacting Fibonacci chain. *Phys. Rev. B* **103**(18), 184205 (2021)
 27. Gudoshnikov, S., Grebenshchikov, Y., Popova, A., Tarasov, V., Gorelikov, E., Liubimov, B.: May. Angle magnetization rotation method for characterizing co-rich amorphous ferromagnetic microwires. *Actuators* **10**(5), 93 (2021)
 28. Meng, F., Li, J., Cushing, S.K., Zhi, M., Wu, N.: Solar hydrogen generation by nanoscale p–n junction of p-type molybdenum disulfide/n-type nitrogen-doped reduced graphene oxide. *J. Am. Chem. Soc.* **135**(28), 10286–10289 (2013)
 29. Blachowicz, T., Ehrmann, A.: Exchange bias in thin films - an update. *Coatings* **11**(2), 122 (2021)
 30. Kiwi, M.: Exchange bias theory. *J. Magn. Magn. Mater.* **234**(3), 584–595 (2001)
 31. Dippong, T., Levei, E.A., Cadar, O., Deac, I.G., Diamandescu, L., Barbu-Tudoran, L.: Effect of nickel content on structural, morphological and magnetic properties of $\text{Ni}_x\text{Co}_{1-x}\text{Fe}_2\text{O}_4/\text{SiO}_2$ nanocomposites. *J. Alloy. Compd.* **786**, 330–340 (2019)
 32. Biswal, S., Bhaskaram, D.S., Govindaraj, G.: Role of graphene oxide in modifying magnetism in $\alpha\text{-Fe}_2\text{O}_3$ nanoparticles: Raman and magnetization studies. *Mater. Chem. Phys.* **266**, 124531 (2021)
 33. Ateia, E.E., El-Nashar, D.E., Ramadan, R., Shokry, M.F.: Synthesis and characterization of EPDM/ferrite nanocomposites. *J. Inorg. Organomet. Polym. Mater.* **30**(4), 1041–1048 (2020)
 34. Shirinova, H.A., Palma, L.D., Sarasini, F.: Synthesis and characterization of magnetic nanocomposites for environmental remediation. *Chem. Eng.* **47**, (2016)
 35. Hovorka, O., Pressesky, J., Ju, G., Berger, A., Chantrell, R.W.: Distribution of switching fields in magnetic granular materials. *Appl. Phys. Lett.* **101**(18), 182405 (2012)
 36. Li, J.R., Tobias, W.G., Matsuda, K., Miller, C., Valtolina, G., De Marco, L., Wang, R.R., Lassablière, L., Quémener, G., Bohn, J.L., Ye, J.: Tuning of dipolar interactions and evaporative cooling in a three-dimensional molecular quantum gas. *Nat. Phys.* 1–5 (2021)
 37. Ateia, E.E., Ateia, M.A., Arman, M.M.: Assessing of channel structure and magnetic properties on heavy metal ions removal from water. *J. Mater. Sci. Mater. Electron.* **33**, 8958–896 (2022)
 38. Nunn, Z.R., Abert, C., Suess, D., Girt, E.: Control of the noncollinear interlayer exchange coupling. *Sci. Adv.* **6**(48), eabd8861 (2020)
 39. Ateia, E.E. and Mohamed, A.T.: Nonstoichiometry and phase stability of Al and Cr substituted Mg ferrite nanoparticles synthesized by citrate method. *J. Magn. Magn. Mater.* **426**, 217–224 (2017)
 40. Lamichhane, T.N., Taufour, V., Palasyuk, A., Bud'ko, S.L., Canfield, P.C.: Study of the ferromagnetic quantum phase transition in $\text{Ce}_{3-x}\text{Mg}_x\text{Co}_9$. *Phil. Mag.* **100**(12), 1607–1619 (2020)
 41. Fialová, S., Pochylý, F.: A new formulation of Maxwell's equations. *Symmetry* **13**(5), 868 (2021)
 42. Ateia, E.E., Ramadan, R., Shafaay, A.S.: Efficient treatment of lead-containing wastewater by CoFe_2O_4 /graphene nanocomposites. *Appl. Phys. A* **126**, 222 (2020)
 43. Ateia, E.E., Ateia, M.A., Fayed, M.G., El-Hout, S., Mohamed, S.G., Arman, M.M.: Synthesis of nanocubic lithium cobalt ferrite toward high-performance lithium-ion battery. *Appl. Phys. A* **128**, 483 (2022)
 44. Mokhosi, S.R., Mdlalose, W., Nhlapo, A., Singh, M.: Advances in the synthesis and application of magnetic ferrite nanoparticles for cancer therapy. *Pharmaceutics* **14**, 937 (2022). <https://doi.org/10.3390/pharmaceutics1405093>

Publisher's Note Springer Nature remains neutral with regard to jurisdictional claims in published maps and institutional affiliations.